Microvascular Research 161 (2025) 104834

Contents lists available at ScienceDirect

Microvascular Research

journal homepage: www.elsevier.com/locate/ymvre

Structural and causal links between retinal vascular geometry and neural layer thickness

Mayinuer Yusufu [a,b], Robert N. Weinreb [c], Mengtian Kang [d], Algis J. Vingrys [a,e], Xianwen Shang [a,b,f], Lei Zhang [a,g], Danli Shi [h,i,j,*], Mingguang He [h,i,j,**]

[a] Centre for Eye Research Australia, Royal Victorian Eye and Ear Hospital, East Melbourne, Australia
[b] Department of Surgery (Ophthalmology), The University of Melbourne, Melbourne, Australia
[c] Hamilton Glaucoma Center, Viterbi Family Department of Ophthalmology and the Shiley Eye Institute, University of California San Diego, La Jolla, CA, USA
[d] Beijing Tongren Eye Center, Beijing Tongren Hospital, Capital Medical University, Beijing 100730, China
[e] Department of Optometry & Visions Sciences, The University of Melbourne, Melbourne, Australia
[f] Guangdong Eye Institute, Department of Ophthalmology, Guangdong Provincial People's Hospital, Guangdong Academy of Medical Sciences, Guangzhou 510080, China
[g] Central Clinical School, Faculty of Medicine, Nursing and Health Sciences, Monash University, Melbourne, Australia
[h] School of Optometry, The Hong Kong Polytechnic University, Kowloon, Hong Kong
[i] Research Centre for SHARP Vision, The Hong Kong Polytechnic University, Kowloon, Hong Kong
[j] Centre for Eye and Vision Research (CEVR), 17W Hong Kong Science Park, Hong Kong

ARTICLE INFO

Keywords:
Retinal vascular geometry
Retina-based microvascular health assessment system
Optical coherence tomography
Retinal layer thickness
Color fundus photography

ABSTRACT

Purpose: To investigate structural relationships between retinal vasculometry from color fundus photography (CFP) and neural layers obtained from Optical Coherence Tomography (OCT) scans.
Methods: This cross-sectional study used the Retina-based Microvascular Health Assessment System (RMHAS) to extract retinal vascular measurements in the 6*6 mm area centered on the macular region and analyzed their associations with OCT parameters. We investigated both pairwise correlations between individual retinal layers and vascular parameters and associations between sets of variables. Mendelian randomization was employed to investigate potential causality.
Results: Data from 67,918 eyes of 43,029 participants were included. Among neural layers, Ganglion Cell-Inner Plexiform Layer (GC-IPL) showed the most notable correlations with vascular Density and Complexity ($r = 0.199$ for arterial Vessel Area Density and $r = 0.175$ for Number of Segments). Inner Nuclear Layer (INL) thickness correlated with Width ($r = 0.122$) and arterial Vessel Area Density ($r = 0.127$). Mendelian randomization indicated a bidirectional causal relationship. Genetically predicted higher Vessel Density was associated with increased thickness across various retinal layers, with standardized effect size of 1.50 on Inner Segment/Outer Segment + Photoreceptor Segment thickness. Genetically predicted increases in retinal layer thicknesses, particularly the Outer Plexiform Layer, were linked to higher Vessel Density (standardized effect size 0.45) and Fractal Dimension (standardized effect size 0.48).
Conclusions: GC-IPL and INL were positively associated with vascular Density and Caliber. Multidimensional relationships indicate a complementary nature between retinal vascular and neural parameters, highlighting their value as a composite biomarker. Mendelian Randomization uncovered a bidirectional causal relationship, providing insights into novel therapeutic approaches targeting vascular and neuronal components.

1. Introduction

The retina, an extension of the central nervous system, provides a distinctive window into human physiology. It enables direct, non-invasive observation of its blood vessels and neural components (Erskine and Herrera, 2014; London et al., 2013), lending itself as a useful indicator for evaluating both ocular and systemic health (Liew et al., 2021; Fu et al., 2023; Yusufu et al., 2024). For instance, retinal

* Correspondence to: D. Shi, School of Optometry, The Hong Kong Polytechnic University, 11 Yuk Choi Road Hung Hom, Kowloon, Hong Kong SAR, China.
** Correspondence to: M. He, School of Optometry, The Hong Kong Polytechnic University, 11 Yuk Choi Road Hung Hom, Kowloon, Hong Kong, SAR, China
E-mail addresses: danli.shi@polyu.edu.hk (D. Shi), mingguang.he@polyu.edu.hk (M. He).

https://doi.org/10.1016/j.mvr.2025.104834
Received 7 April 2025; Received in revised form 23 May 2025; Accepted 22 June 2025
Available online 27 June 2025

vascular features, including vessel diameter, tortuosity, and branching patterns, quantified from color fundus photography (CFP), have been associated with cardiovascular diseases, diabetes, and hypertension (Tien Yin Wong et al., 2001; Sasongko et al., 2010). Retinal layer measurements such as retinal nerve fiber layer (RNFL) thickness and ganglion cell-inner plexiform layer (GC-IPL) thickness derived from Optical Coherence Tomography (OCT) have shown associations with neurodegenerative diseases like Alzheimer's disease, Parkinson's disease, and multiple sclerosis (Chan et al., 2019; Satue et al., 2016; Petzold et al., 2017).

While previous studies have explored associations between retinal features and various systemic conditions, they primarily focused on studying retinal vascular and neural features separately. There is a gap in our understanding of the relationships between the information provided by those two modalities. Although the development of artificial intelligence has empowered their detailed quantification and facilitated the differentiation of subtle retinal feature alterations (Shi et al., 2022; Ko et al., 2017), there is a paucity of information about detailed associations between vascular features observed in CFP and neural characteristics measured by OCT.

CFP and OCT offer complementary data on vascular and neural health, respectively. Notably, the functional interplay between retinal vessels and neurons and ganglion cells, known as neurovascular coupling, plays an essential role in maintaining normal retinal physiology and is disrupted in many ocular diseases, such as diabetic retinopathy and glaucoma (Wareham and Calkins, 2020; Gardner and Davila, 2017), and by extension, brain function (Girouard and Iadecola, 2006). In addition, their interrelationship could provide a more comprehensive understanding of retinal physiology and pathology, as well as the underlying pathophysiology of conditions involving both vascular and neural health. Such insights could lead to the identification of early composite markers of neurodegeneration and vascular cognitive impairment, facilitating earlier diagnosis and intervention in conditions such as Alzheimer's disease (Czako et al., 2020; Normando et al., 2016).

In the current study, we aim to bridge this gap by investigating structural relationships between retinal vasculometry obtained from CFPs and OCT-derived retinal layer parameters in a large cohort of participants from the UK Biobank. In addition, this study aims to further unveil the causal relationship between retinal vascular and neural features through Mendelian Randomization.

2. Methods

2.1. Study design and population

For the correlation analyses in this cross-sectional study, we used unidentifiable data from the UK Biobank. The UK Biobank study is a large population-based cohort study that enrolled participants aged 40 to 69 years that was launched in 2006 in the United Kingdom, and introduced eye examinations in 2009, including CFP (Sudlow et al., 2015; Chua et al., 2019). The UK Biobank cohort study obtained ethical approval from the North West Multi-Centre Research Ethics Committee (reference number 06/MRE08/65).

2.2. Retinal vascular measurements

The retinal vascular parameters were obtained using Retina-based Microvascular Health Assessment System (RMHAS) (Shi et al., 2022) from a 6*6 mm area centered on the macular region of CFPs. The detailed description of vascular measurements has been previously published (Yusufu et al., 2025). In brief, the RMHAS automatedly segmented and quantified measurements of 5 categories: Calibers, Density, Tortuosity, Branching Angle, and Complexity, and in this study, 23 measurements in the macular region were used. Supplementary Table 1 presents the detailed definition and classification of vascular measurements. Fig. 1 shows the corresponding structure of the retinal vascular network obtained from CFPs and cross-sectional layers obtained from OCT scans in the 6*6 mm area.

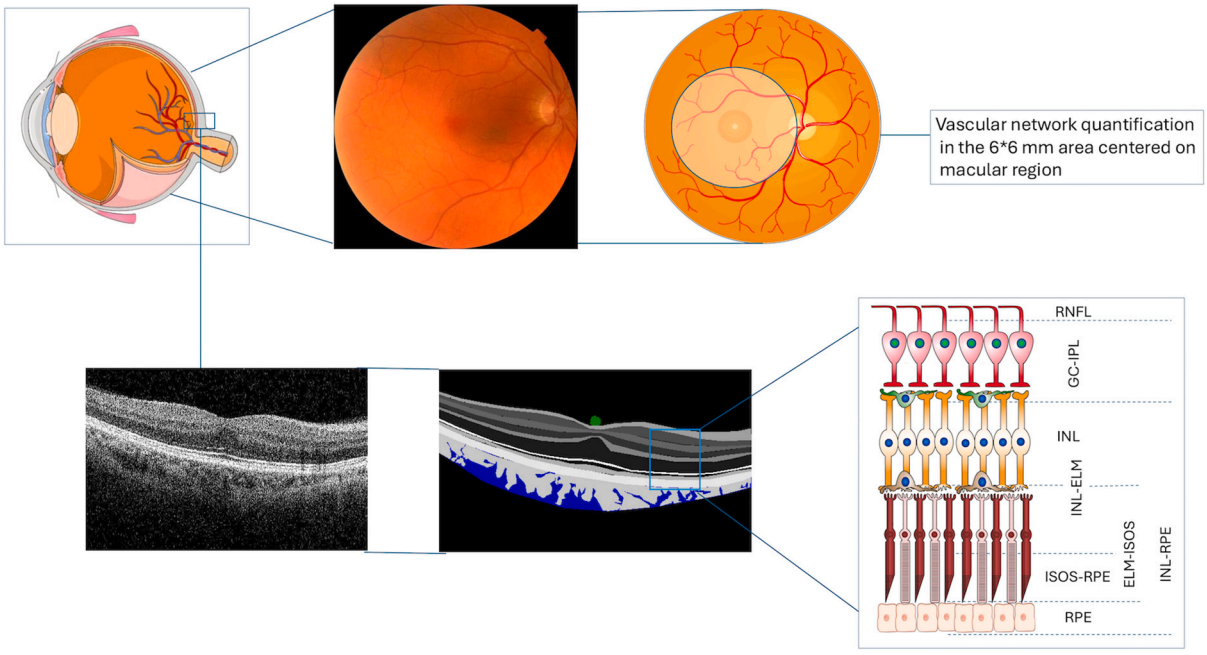

Fig. 1. Two imaging modalities of retina structures.
Notes: This figure used image provided by Servier Medical Art (https://smart.servier.com/), licensed under CC BY 4.0 (https://creativecommons.org/licenses/by/4.0/), from Elisa Galliano. Retina circuit. DOI: https://doi.org/10.5281/zenodo.4756818 from SciDraw licensed under CC BY 4.0, and Chilton, J. (2020). Ependymal cell.Zenodo. https://doi.org/10.5281/zenodo.3926497 from SciDraw licensed under CC BY 4.0. Abbreviations: RNFL, retinal nerve fiber layer; GC-IPL, ganglion cell layer-inner plexiform layer; INL, inner nuclear layer; ELM, external limiting membrane; ISOS, inner segment/outer segment; RPE, retinal pigment epithelium.

2.3. OCT parameters

Measurements of neural layer thickness were extracted using Topcon Advanced Boundary Segmentation (TABS) software by Ko F. et al., with 8 quality control measures generated (Ko et al., 2017; Yang et al., 2010). After removing parameters with >30 % missing values and keeping only parameters presenting retinal layer thickness of the 6*6 mm area, we included 9 parameters: macular thickness, RNFL, GC-IPL, inner nuclear layer (INL), INL-retinal pigment epithelium (RPE), INL-external limiting membrane (ELM), ELM-inner segment/outer segment (ISOS), ISOS-RPE, and RPE thickness. Fig. 1 shows the representative OCT cross-sectional image alongside an illustrative schematic of these segmented retinal layers.

2.4. Inclusion and exclusion criteria

We excluded participants who withdrew their consent or did not have CFPs and/or OCT data. The quality of the CFPs was assessed with

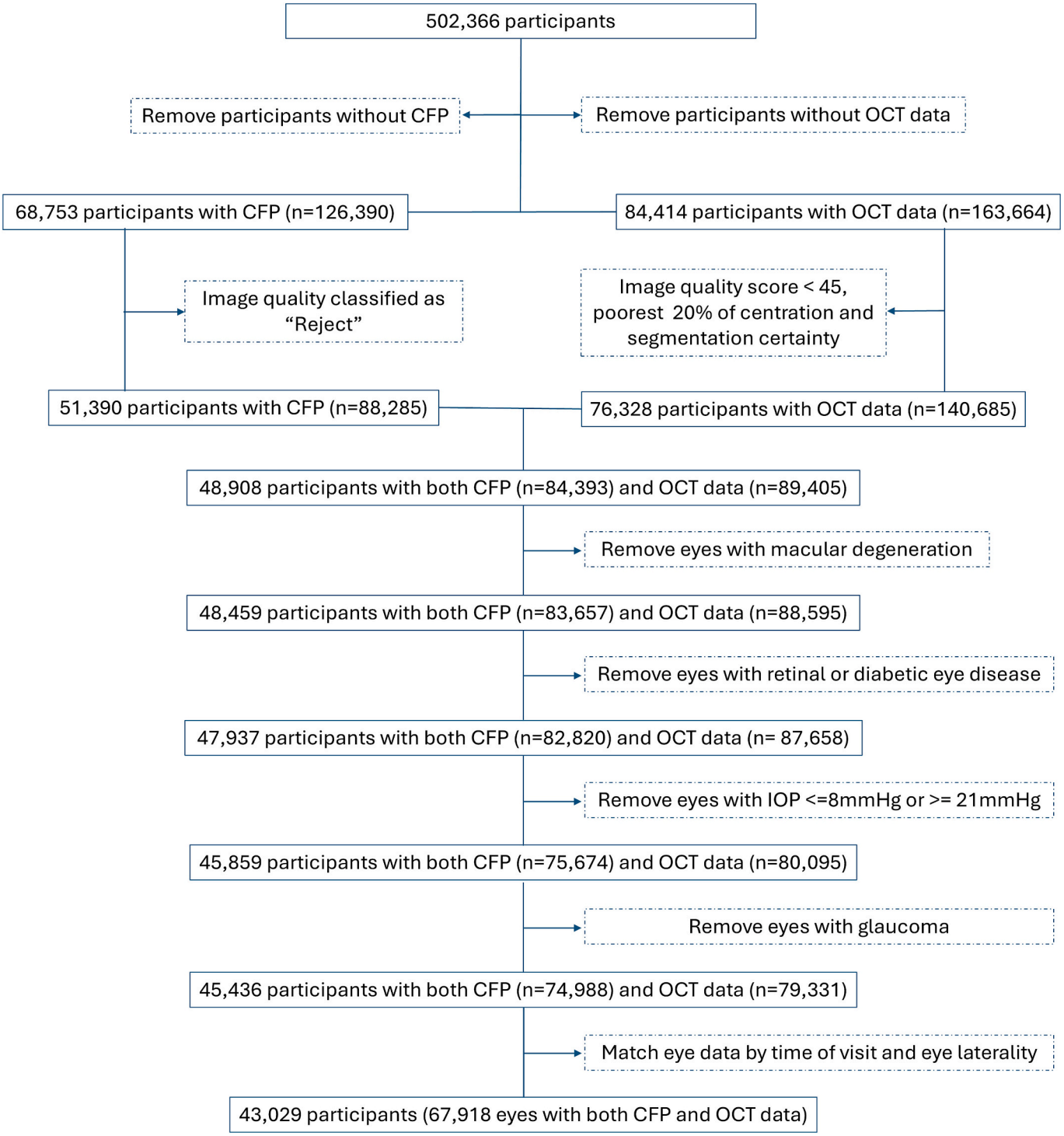

Fig. 2. Participants selection process.
Notes: OCT, Optical Coherence Tomography. CFP, Color Fundus Photograph. Definitions of variables used in the selection process are presented in Supplementary Table 2.

RMHAS, and those classified as "Reject" were removed (Shi et al., 2022). The quality of OCT data was assessed using the quality control indicators obtained with the Topcon Advanced Boundary Segmentation software (Patel et al., 2016). For image quality control, we followed the criteria used by Ko F. et al (Ko et al., 2017). Lastly, we excluded eyes with conditions that could potentially affect vascular network quantification or retinal layer thickness measurements. These included intraocular pressure (IOP) of $\geq$21 mmHg or $\leq$ 8 mmHg, self-reported glaucoma, macular degeneration, retinal diseases, diabetic eye diseases, or history of glaucoma surgery (Ko et al., 2017). Fig. 2 shows the inclusion and exclusion at each stage. Definitions of variables are presented in Supplementary Table 2.

2.5. Mendelian randomization

We performed a bidirectional, two-sample Mendelian Randomization to examine further the potential causal relationship between vascular network features and retinal layer thickness. For the vascular features, we used single nucleotide polymorphisms (SNPs) of retinal vascular network features obtained in the UK Biobank (Zekavat et al., 2022). The study (Zekavat et al., 2022) provided genome-wide association study (GWAS) data on retinal Vessel Density and Fractal Dimension. For the retinal layer thickness, we used GWAS data of retinal layer thickness obtained from the Leipzig Research Centre for Civilization Diseases (LIFE-Adult Study) (Zekavat et al., 2024; Loeffler et al., 2015). Details of GWAS studies can be found in Supplementary Text 1. The baseline of the LIFE-Adult Study was carried out from August 2011 to November 2014 in Leipzig, Germany, focusing on investigating prevalences, early onset markers, genetic predispositions, and lifestyle determinants of major civilization diseases in participants aged 40–79 (Loeffler et al., 2015).

2.6. Statistical analysis

To describe baseline characteristics, we summarized continuous variables with mean (standard deviation [SD]), while categorical variables were presented as counts and percentages. We removed outliers using the method proposed by Zekayat et al (Zekavat et al., 2022). Parameters with a missing proportion of >30 % were excluded. Missing values were imputed using Multivariate Imputation by Chained Equations. To ensure comparability, all measurements were rescaled to the SD unit.

We assessed normality of the data distribution with the Anderson-Darling test. For the correlation test, we used Pearson correlation if both variables were normally distributed, otherwise Spearman's rank correlation was used. Benjamini-Hochberg was used to adjust for false discovery. We generated a heatmap based on the correlation matrix to assess the pairwise strength and direction of the relationships between all possible pairs of retinal vessel characteristics and OCT parameters.

For broader structural relationships between these two sets of variables, we employed Canonical Correlation Analysis (CCA). The CCA generates dimensions that are linear combinations of variables from each set that maximize the correlation between the two sets. The proportion of variance explained by each canonical dimension was calculated to assess the relative importance of each dimension in explaining the overall relationship between the two sets of variables. The scatter plot with a fitted locally estimated scatterplot smoothing (LOESS) curve and linear regression line illustrated the correlation in the canonical dimensions. A Sankey diagram was constructed to depict the change in variable importance across canonical dimensions.

For the bidirectional Mendelian Randomization, SNPs with a GWAS-correlated *P*-value $<5 \times 10^{-6}$ were selected, and data clumping was performed with the linkage disequilibrium r^2 set at 0.001 and clumping

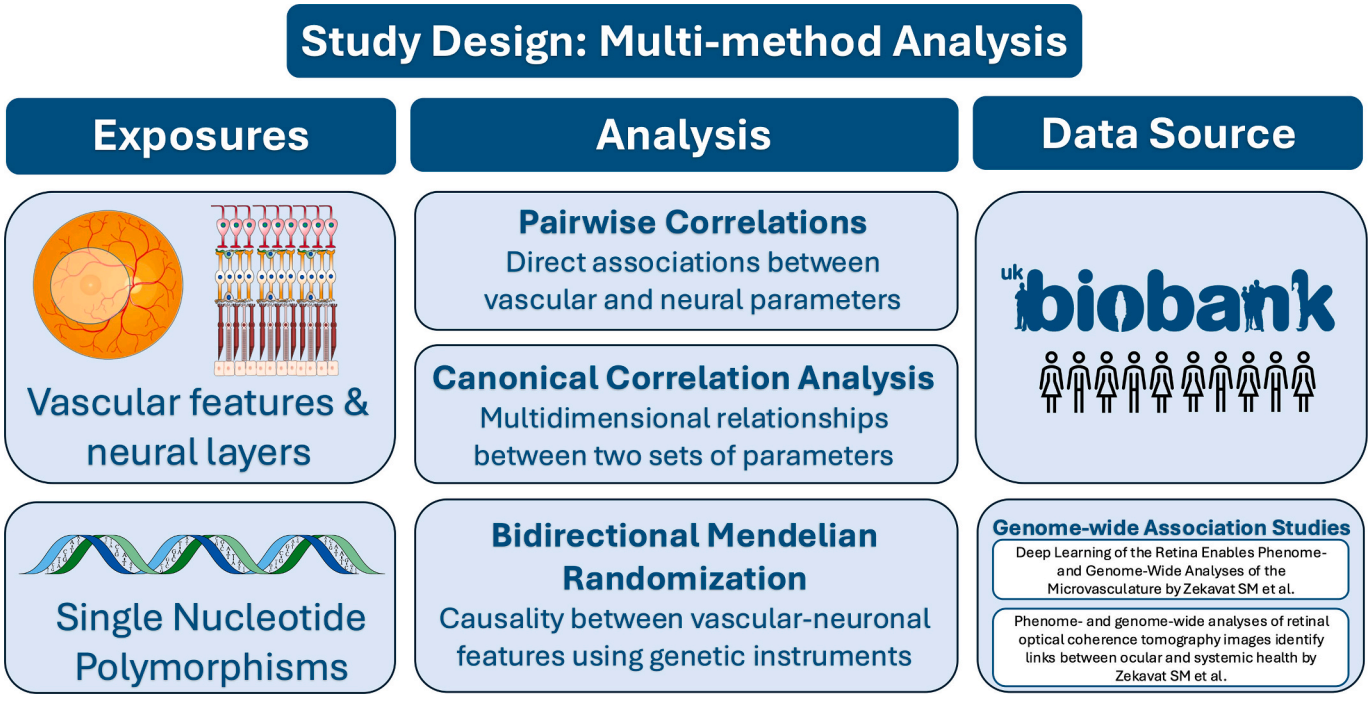

Fig. 3. Study Design.
Notes: This figure used image provided by Servier Medical Art (https://smart.servier.com/), licensed under CC BY 4.0 (https://creativecommons.org/licenses/by/4.0/), from Elisa Galliano. Retina circuit. DOI: https://doi.org/10.5281/zenodo.4756818 from SciDraw licensed under CC BY 4.0, Chilton, J. (2020). Ependymal cell.Zenodo. https://doi.org/10.5281/zenodo.3926497 from SciDraw licensed under CC BY 4.0, and Vivek Kumar. DNA. DOI: https://doi.org/10.5281/zenodo.4072322 from SciDraw licensed under CC BY 4.0. Data sources for Mendelian Randomization: Zekavat SM, Raghu VK, Trinder M, et al. Deep Learning of the Retina Enables Phenome- and Genome-Wide Analyses of the Microvasculature. Circulation. Jan 11 2022;145(2):134–150. doi:https://doi.org/10.1161/circulationaha.121.057709, and Zekavat SM, Jorshery SD, Rauscher FG, et al. Phenome- and genome-wide analyses of retinal optical coherence tomography images identify links between ocular and systemic health. Sci Transl Med. Jan 24 2024;16(731):eadg4517. doi:https://doi.org/10.1126/scitranslmed.adg4517.

window set at 10000 kb. To ensure the comparability among parameters, the standardized effect sizes were presented.

Fig. 3 shows the design of this multi-method approach. Additionally, to assess the robustness and consistency of the correlations, we conducted several subgroup and sensitivity analyses. Specifically, correlations were examined by sex and age groups (Supplementary Tables 3–4), as well as by eye laterality (Supplementary Table 5). To address potential within-subject correlation, additional sensitivity analyses were performed by selecting only one eye per participant (Supplementary Table 6). Finally, to explore potential non-linear relationships, we categorized vascular and thickness parameters into quintiles and assessed correlations between these categorical variables (Supplementary Table 7). In this study, a two-sided significance level of alpha = 0.05 was set for all statistical tests. All analyses were conducted using R version 4.2.3.

3. Results

3.1. Characteristics of participants

Starting with 502,366 participants, our selection process filtered for those with both CFP and OCT data but excluded low-quality images and data and eyes with conditions that would affect the segmentation and quantification of retinal features. Our final cohort was 43,029 participants with 67,918 eyes that had both quality CFP and OCT data.

The mean (SD) age of the participants was 55.5 (8.19) years, with a higher proportion of females (55.6 %) than males (44.4 %) and males being slightly older than females (55.7 vs 55.3 years, $p < 0.001$). Males had a higher mean body mass index (27.6 vs 26.7 kg/m^2, $p < 0.001$) and were more likely to be current or former smokers (47.1 % vs 38.2 %, $p < 0.001$) compared with females. Males also reported higher levels of physical activity, with 36.0 % in the high category compared with 30.6 % of females ($p < 0.001$). Cardiovascular risk factors showed significant differences across genders, with males having higher mean SBP (138 vs 133 mmHg, p < 0.001), DBP (83.2 vs 79.8 mmHg, p < 0.001), and HbA1c levels (35.8 vs 35.3 mmol/mol, p < 0.001). Females had higher mean high-density lipoprotein (1.63 vs 1.31 mmol/L, p < 0.001) and low-density lipoprotein (3.59 vs 3.51 mmol/L, p < 0.001) levels. The prevalence of diabetes (4.9 % vs 2.8 %, p < 0.001) and cardiovascular diseases (29.9 % vs 21.3 %, $p < 0.001$) was higher in males. Detailed characteristics of participants stratified by sex can be found in Table 1.

3.2. Pairwise correlations

Fig. 4 illustrates the pairwise correlations between retinal vascular features and the thickness of retinal layers. Macular thickness had moderate positive correlations with multiple vascular features, particularly the Density measure. The highest correlations were observed for arterial Vessel Area Density ($r = 0.161$, $p < 0.001$), arterial Vessel Skeleton Density ($r = 0.132$, p < 0.001), and Width ($r = 0.118$, p < 0.001). Similarly, GC-IPL demonstrated comparatively higher positive correlations with these vascular features, most notably with arterial Vessel Area Density ($r = 0.199$, $p < 0.001$), arterial Vessel Skeleton Density ($r = 0.170$, $p < 0.001$), and venular Vessel Skeleton Density ($r = 0.152$, $p < 0.001$). INL also showed positive correlations with several vascular features, such as Width ($r = 0.122$, p < 0.001) and arterial Vessel Area Density ($r = 0.127$, $p < 0.001$).

GC-IPL thickness was also positively associated with Complexity measures, such as Number of Segments ($r = 0.175$, $p < 0.001$) and Number of Branching ($r = 0.157$, p < 0.001). Conversely, the Length Diameter Ratio (LDR) showed negative correlations with multiple retinal layer thicknesses, particularly GC-IPL ($r = -0.143$, p < 0.001) and INL ($r = -0.106$, p < 0.001). RNFL showed generally weaker correlations, with the strongest observed correlation being a relatively weak positive correlation with arterial Vessel Skeleton Density ($r = 0.065$, p < 0.001). Most correlations were statistically significant (p <

Table 1
Baseline characteristics of participants.

Characteristic	Whole Sample ($N = 43,029$)	Female ($N = 23,917$)	Male ($N = 19,112$)	P-value
Age (years)				<0.001
Mean (SD)	55.5 (8.19)	55.3 (8.02)	55.7 (8.38)	
Body Mass Index (kg/m^2)				<0.001
Mean (SD)	27.1 (4.69)	26.7 (5.09)	27.6 (4.10)	
Missing, N (%)	202 (0.5 %)	107 (0.4 %)	95 (0.5 %)	
Smoking Status, N (%)				<0.001
Never	24,664 (57.3 %)	14,665 (61.3 %)	9999 (52.3 %)	
Previous	14,191 (33.0 %)	7264 (30.4 %)	6927 (36.2 %)	
Current	3940 (9.2 %)	1862 (7.8 %)	2078 (10.9 %)	
Missing	234 (0.5 %)	126 (0.5 %)	108 (0.6 %)	
Physical Activity, N (%)				<0.001
Low	6107 (14.2 %)	3184 (13.3 %)	2923 (15.3 %)	
Moderate	14,124 (32.8 %)	8027 (33.6 %)	6097 (31.9 %)	
High	14,199 (33.0 %)	7310 (30.6 %)	6889 (36.0 %)	
Missing	8599 (20.0 %)	5396 (22.6 %)	3203 (16.8 %)	
Systolic Blood Pressure (mmHg)				<0.001
Mean (SD)	135 (18.0)	133 (18.6)	138 (16.6)	
Missing, N (%)	144 (0.3 %)	90 (0.4 %)	54 (0.3 %)	
Diastolic Blood Pressure (mmHg)				<0.001
Mean (SD)	81.3 (9.98)	79.8 (9.92)	83.2 (9.74)	
Missing, N (%)	144 (0.3 %)	90 (0.4 %)	54 (0.3 %)	
Glycated Haemoglobin (mmol/mol)				<0.001
Mean (SD)	35.6 (5.79)	35.3 (5.19)	35.8 (6.44)	
Missing, N (%)	5127 (11.9 %)	2938 (12.3 %)	2189 (11.5 %)	
High-Density Lipoprotein (mmol/L)				<0.001
Mean (SD)	1.49 (0.387)	1.63 (0.382)	1.31 (0.312)	
Missing, N (%)	5742 (13.3 %)	3383 (14.1 %)	2359 (12.3 %)	
Low-Density Lipoprotein (mmol/L)				<0.001
Mean (SD)	3.55 (0.852)	3.59 (0.853)	3.51 (0.849)	
Missing, N (%)	3677 (8.5 %)	2117 (8.9 %)	1560 (8.2 %)	
Diabetes, N (%)				<0.001
No	41,205 (95.8 %)	23,141 (96.8 %)	18,064 (94.5 %)	
Yes	1589 (3.7 %)	662 (2.8 %)	927 (4.9 %)	
Missing	235 (0.5 %)	114 (0.5 %)	121 (0.6 %)	
CVD, N (%)				<0.001
No	32,024 (74.4 %)	18,709 (78.2 %)	13,315 (69.7 %)	
Yes	10,813 (25.1 %)	5097 (21.3 %)	5716 (29.9 %)	
Missing	192 (0.4 %)	111 (0.5 %)	81 (0.4 %)	

Notes: SD: standard deviation; N, number; CVD, Cardiovascular Disease. For differences between groups, we used *t*-tests for normally distributed numerical data and Wilcoxon rank–sum tests if numerical data were not normally distributed. For categorical data, we used $\chi 2$ test.

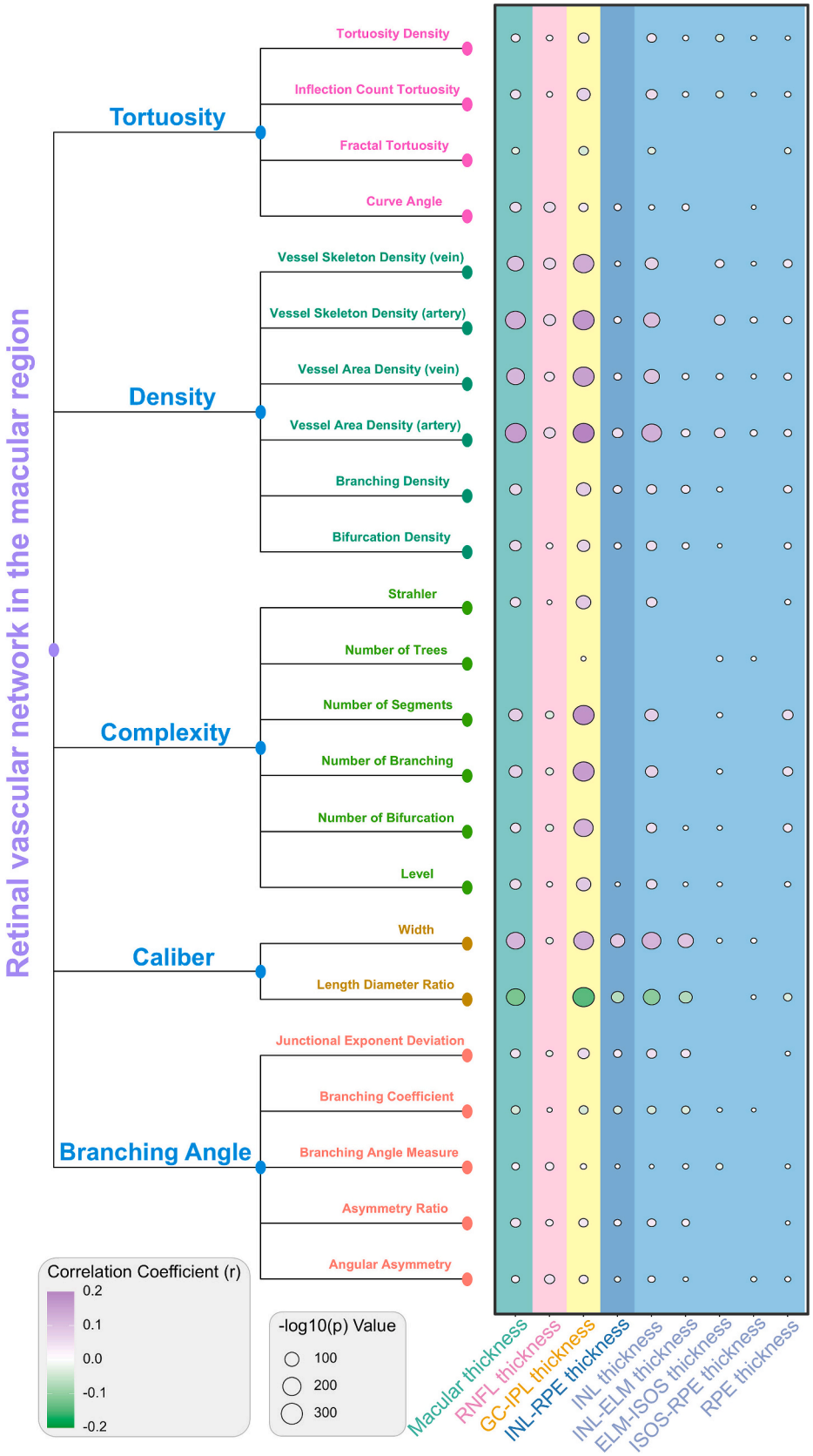

Fig. 4. Correlations between retinal vascular features and thickness of retinal layers.
Notes: Circle size represents statistical significance (−log10(p) value), while its color indicates the strength and direction of correlation (purple for positive, green for negative). Only those correlations with $p < 0.05$ after FDR adjustment were presented with a circle. Abbreviations: RNFL, retinal nerve fiber layer; GC-IPL, ganglion cell-inner plexiform layer; INL, inner nuclear layer; ELM, external limiting membrane; ISOS, inner segment/outer segment; RPE, retinal pigment epithelium; FDR, false discovery rate. The calculated correlation coefficients and the corresponding *p*-values can be found in Supplementary Table 8.

0.001), although the strength of these correlations was mostly modest.

3.3. Canonical correlation analysis

Fig. 5 shows the main results of CCA. The sharp increase in cumulative variance observed in the first three dimensions suggests that most of the important relationships between the two sets of variables are captured. The first canonical dimension explained approximately 43.8 % of the variance in the relationship between retinal vascular and OCT parameters, and subsequent dimensions contributed 29.88 %. Taken together, the first three dimensions collectively account for over 92.02 % of the total variance explained.

The first canonical dimension showed a moderate positive correlation ($\rho = 0.265$) between retinal vascular measurements and retinal layer thickness. The correlation coefficients were 0.218 and 0.171 in the second and third dimensions (all $p < 0.001$). In the scatter plots of the first three canonical dimensions, the LOESS curves largely overlapped with the fitted linear lines, suggesting predominant linear relationships with merely weak non-linear relationships at the extremes of the distributions.

The Sankey diagram revealed distinct patterns of variable importance across four canonical dimensions, highlighting the complex relationships between structural OCT parameters and vascular characteristics. In the first dimension, the number of segments, GC-IPL thickness, and INL-RPE thickness appeared to be the most influential variables. The second dimension showed a transition toward vascular dominance, with arterial Vessel Area Density, Junctional Exponent Deviation (JED), and INL-ELM thickness as the major contributors. The third and fourth dimensions displayed more evenly distributed patterns of variable importance, with contributions from parameters such as vessel width, branching patterns, and various layer thicknesses. In the third dimension 3, vascular parameters, such as Width, arterial Vessel Skeleton Density, and branching characteristics emerged as important contributors, suggesting a different aspect of retinal architecture captured by this dimension. (Supplementary Figs. 1 and 2), while dimension 4 demonstrated unique patterns with RPE, INL-RPE, and several vascular density measurements showing high importance.

3.4. Mendelian randomization

Table 2 presents the results of bidirectional Mendelian randomization, revealing significant associations of various retinal layers with Vessel Density and Fractal Dimension. Vessel Density showed the strongest effect on ISOS + Photoreceptor Segment (ISOS+PS) thickness, with a standardized effect size of 1.50 (95 % CI: 1.07, 1.93; $p < 0.001$). In addition, Vessel Density also showed significant positive effects on Ganglion Cell Layer (GCL) and Outer Plexiform Layer (OPL) thicknesses, with standardized effect sizes of 0.50 and 0.57 (both p-values <0.05). When examining the effect of layer thickness on Vessel Density, multiple retinal layer thicknesses exhibited significant effects. OPL thickness demonstrated the largest effect on Vessel Density, with an effect size of 0.45 (95 % CI: 0.16, 0.75, $p = 0.002$). GCC, GCL, ISOS+PS, and INL thicknesses also significantly positively affected Vessel Density, with effect sizes ranging from 0.27 to 0.40 (all $p < 0.05$). While Mendelian randomization did not demonstrate the effect of Fractal Dimension on the thickness of layers, the reverse effect was revealed. GCC, GCL, IPL, OPL, and INL all showed significant effects, with standardized effect sizes ranging between 0.25 and 0.48.

4. Discussion

We conducted a comprehensive analysis of the relationships between retinal layer thicknesses and vascular features in 67,918 eyes of 43,029 participants by evaluating pairwise correlations, correlations between two sets of parameters, and their genetic influence on each other. Among neural layers, the GC-IPL and INL showed the most notable associations with vascular features, including Density, Complexity, and Caliber measurements, with relatively higher correlations observed for arteries than veins. The CCA results further revealed multidimensional relationships between the two sets of parameters, indicating a complementary nature of their relationships. Furthermore, the Mendelian Randomization analysis suggested evidence for bidirectional causal relationships.

The pairwise correlation analysis revealed the most notable correlations for GC-IPL with arterial Vessel Area Density and arterial Vessel Skeleton Density, Number of Segments, Number of Branching, and Number of Bifurcation. This finding is consistent with previous research revealing decreased vascular density obtained with OCT Angiography (OCTA) was associated with thinner ganglion cell complex (Takusagawa et al., 2017). The Mendelian Randomization also revealed the effect of Vessel Density on GCL, suggesting richer macular blood supply supports enhanced growth of ganglion cells. Given the high metabolic demand of ganglion cell bodies and dendrites in the GC-IPL, its thickness is critically dependent on adequate blood supply (Kur et al., 2012; Iadecola, 2013; Ames 3rd., 2000), explaining the relatively higher correlation found for arterial Density parameters compared with venular Density parameters. Increased metabolic demand may also induce vascular remodeling, such as increased bifurcations to facilitate efficient nutrient delivery and waste removal (Kur et al., 2012). In addition, increased neural activity in the GC-IPL may stimulate the release of vasoactive signals (e.g., nitric oxide, vascular endothelial growth factor), promoting angiogenesis and vascular bifurcation (Attwell et al., 2010a).

INL thickness was another layer primarily contributing to the correlations between vascular features and macular thickness. INL thickness was positively correlated with Width ($r = 0.122$) and negatively correlated with LDR ($r = -0.106$). This might indicate that thinner INL was associated with a narrower diameter and elongated vessels relative to their diameter. Such a geometric pattern could potentially reflect vascular remodeling in response to altered metabolic demands or could be an early sign of microvascular dysfunction (Broe et al., 2014). Previous studies have shown that changes in vessel morphology, including alterations in LDR, can be indicative of various retinal pathologies and systemic conditions such as diabetes and hypertension (Hughes et al., 2009). In addition, we found INL was associated with Vessel Area Density. This is consistent with the findings in a previous study (Yu et al., 2016), which proposed the retinal vascular network had a more important role for the inner retina, while the oxygen and nutrition supply of the outer retina could rely on the choroid (Kur et al., 2012).

The CCA revealed that the first three canonical dimensions explained >90 % of the variance. The parameters that showed comparatively notable correlations in the pairwise correlation analysis also primarily contributed to the correlations between the two sets of parameters. The first canonical dimension, explaining 43.8 % of the variance, revealed a positive correlation ($\rho = 0.265$). This modest correlation suggests that these two sets of measurements provide complementary rather than redundant information about retinal health and structure. This is partially supported by a previous study that reported that the combined use of CFP and OCT biomarkers led to improved performance for predicting late age-related macular degeneration development (Wu et al., 2021). This highlights the value of the retinal vascular and neural layer as a composite biomarker. The Sankey diagram (Fig. 5C) highlighted the complex relationships between structural OCT parameters and vascular characteristics with distinct patterns of the relationship across the first four canonical dimensions. These findings suggested that neither OCT parameters nor vascular metrics should be considered in isolation. This comprehensive understanding of structure-vessel relationships may guide future research into diagnostic and therapeutic strategies for retinal diseases. Nonetheless, longitudinal and disease-specific validation is required to clarify the clinical relevance of these findings. Further research should extend the application of grouped retinal vascular and neural biomarkers to systemic disease prediction. The information obtained on retinal vascular architecture and neural status especially may

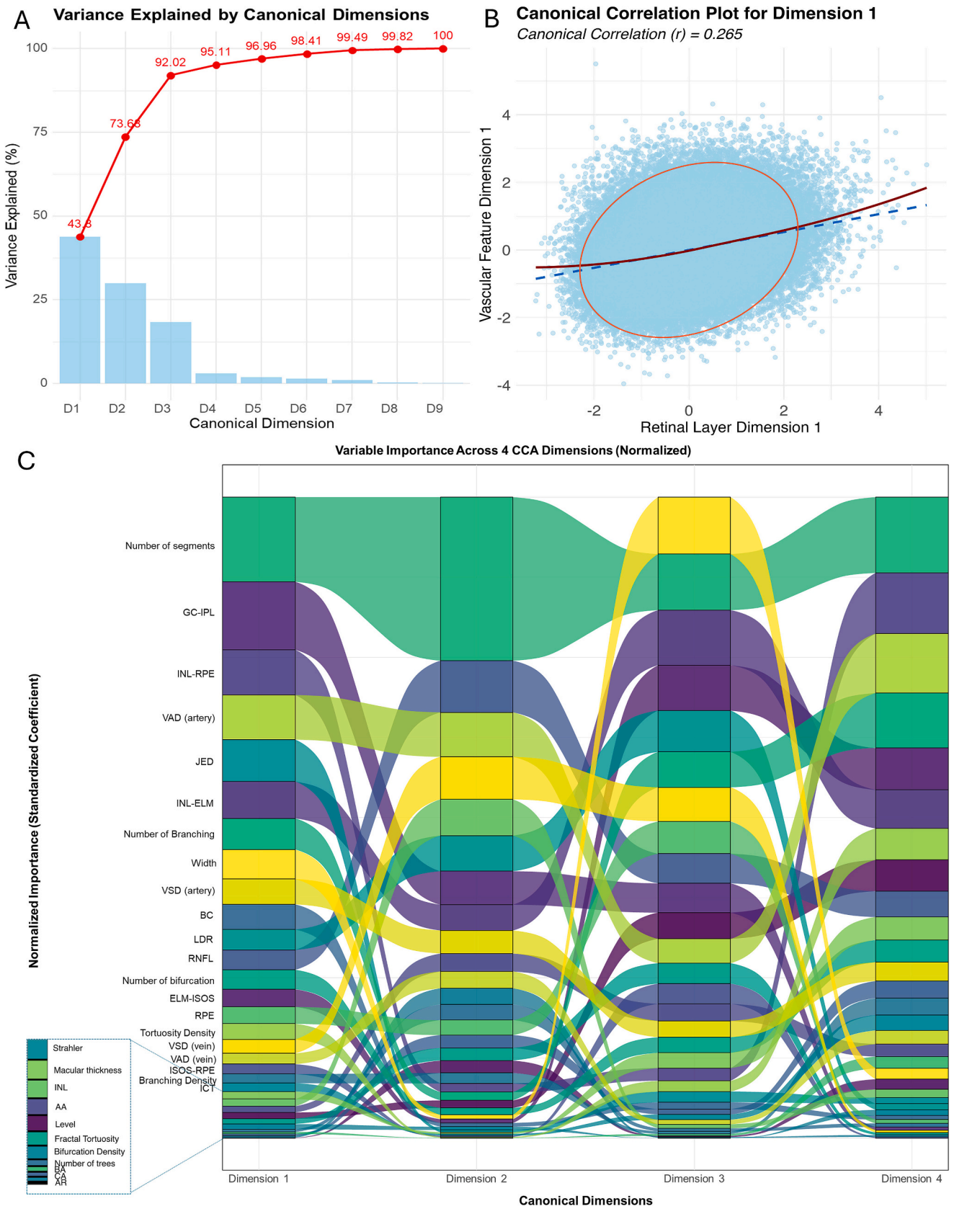

(caption on next page)

Fig. 5. Canonical Correlation Analysis (CCA) of Retinal Vascular Measurements and Retinal Layer Thickness.
Notes: (A) Variance Explained: The bar chart (blue) shows the proportion of variance explained by each canonical dimension, while the line graph (red) displays the cumulative variance explained. D stands for dimension. This illustrates the relative importance of each dimension in capturing the relationship between retinal vascular and OCT parameters. The first four dimensions explained over 95 % of the variance. (B) First Canonical Dimension Correlation: This scatter plot depicts the correlation between the first canonical variates for retinal vascular measurements (y-axis) and retinal layer thickness (x-axis). The red ellipse outlines the 95 % confidence region of the data distribution. The blue dashed line shows the linear regression fit, while the solid red curve represents the locally estimated scatterplot smoothing (LOESS) fit, providing a non-linear visualization of the relationship. The canonical correlation (ρ) of 0.265 indicates the strength of the association for this dimension. (C) Variable Importance Across Dimensions: This Sankey diagram illustrates how the importance of different variables (both retinal vascular measurements and OCT parameters) changed across the first four canonical dimensions. The height of each flow represents the magnitude of a variable's contribution to each dimension, allowing for the visualization of which variables are most influential in each canonical relationship. Supplementary Figs. 1 and 2 show the correlations of the first four dimensions and the loadings of variables.

Table 2
Bidirectional Mendelian Randomization.

Exposure	Outcome	Method	NSNPs	Standardized Effect Size (95 % CI)	P-value
VD	ISOS+PS	Wald ratio	1	1.50 (1.07, 1.93)	<0.001
VD	GCL	Wald ratio	1	0.50 (0.10, 0.89)	0.015
VD	OPL	Wald ratio	1	0.57 (0.37, 0.78)	<0.001
OPL	VD	IVW	3	0.45 (0.16, 0.75)	0.002
GCC	VD	IVW	2	0.27 (0.12, 0.41)	<0.001
ISOS+PS	VD	IVW	2	0.28 (0.20, 0.35)	<0.001
GCL	VD	IVW	3	0.40 (0.06, 0.75)	0.019
INL	VD	Wald ratio	1	0.39 (0.32, 0.46)	<0.001
IPL	VD	IVW	2	0.43 (−0.02, 0.87)	0.06
GCL	FD	IVW	2	0.44 (0.29, 0.58)	<0.001
INL	FD	Wald ratio	1	0.25 (0.18, 0.32)	<0.001
GCC	FD	Wald ratio	1	0.32 (0.19, 0.46)	<0.001
IPL	FD	Wald ratio	1	0.44 (0.32, 0.56)	<0.001
OPL	FD	Wald ratio	1	0.48 (0.35, 0.61)	<0.001

Notes: SNP, single nucleotide polymorphism; NSNPs, number of SNPs; VD, Vessel Density; FD, Fractal Dimension; OPL, outer plexiform layer; GCC, ganglion cell complex; ISOS, inner segment/outer segment; PS photoreceptor segments; GCL, ganglion cell layer; INL, inner nuclear layer; GCC included RNFL, GCL, and inner plexiform layer. ISOS+PS included external limiting membrane-ISOS + ISOS-retinal pigment epithelium; IVW, Inverse variance weighted. When only one SNP was identified for each pair of exposure and outcome, the Wald ratio was used, while if more than one was identified, then IVW was used. The standardized effect size was calculated to represent the change in the outcome variable (in SD units) for a one-unit change in the exposure variable.

be relevant to changes in brain functions (Cabrera DeBuc et al., 2018) and potentially could serve as early biomarkers.

The bidirectional relationships revealed by Mendelian randomization analyses point to shared genetic influences between retinal vascular features and retinal layer thicknesses. This genetic overlap suggests common developmental pathways and regulatory mechanisms governing both vascular and neuronal components of the retina. A previous study reported that genes and signaling pathways, such as the Norrin signaling pathway mediated by the FZD4/LRP5/TSPAN12 receptor complex, involved in angiogenesis and neurogenesis during retinal development may have pleiotropic effects, influencing vascular architecture and neuronal layer formation (Selvam et al., 2018). Additionally, the correlation between ganglion cell complex and vessel density aligns with fundamental embryological principles. During early retinal development, axons of retinal ganglion cells serve as guidance pathways for developing blood vessels, with nerve fiber layer formation preceding vascularization (Edwards et al., 2012). Previous research suggested the intricate bidirectional interaction between retinal vascular health and blood supply regulation is closely linked to the integrity of retinal neurons and neural activity (Pournaras et al., 2008; Iadecola, 2017; Attwell and Iadecola, 2002; Attwell et al., 2010b), providing additional evidence on neurovascular coupling in the retina in terms of phenotypic morphology and genetics. Furthermore, the consistent associations across multiple retinal layers and vascular features indicate that these shared genetic factors may have broad effects on retinal structure and function.

Our study presents several strengths including large sample size, inclusion of a wide range of retinal vessel and neural layer features, and the employment of advanced statistical methods including CCA and Mendelian randomization. In addition, our study established baseline associations between retinal vascular geometrics and neural layer thickness in healthy individuals, which could also lay the groundwork for understanding early pathological changes in diseased status. The bidirectional relationships suggest the presence of shared genetic influences and developmental pathways between vascular and neuronal components of the retina. This knowledge could lead to new therapeutic targets for ocular conditions affecting both neurological and vascular health. For instance, future studies could explore whether interventions targeting vascular health—such as improving perfusion or reducing vascular resistance—could enhance ganglion cell survival and function in conditions like glaucoma or diabetic retinopathy. In addition, our results revealed the bidirectional, multi-dimensional, complementary nature between retinal neuro-vascular interactions. These results suggested that the integration of vascular features and neural layer thickness could provide early composite biomarkers for neurovascular conditions.

Despite its strengths, our study has some limitations. First, the analyses were performed in the population with a majority being Caucasians, which may affect the generalizability of the findings. Additionally, due to the low availability of GWAS data on OCT-derived retinal layers, we used data from a replication study in LIFE-Adult-study. Therefore, the SNPs included may not be all SNPs that can be identified in this study population. Additionally, our study focused specifically on retinal layer thickness, which represents only one aspect of neural characteristics. Future studies incorporating additional neural parameters, such as ganglion cell density measurements and dendritic arborization patterns, could provide more detailed neural characterization to complement our findings.

In conclusion, we revealed that macular thickness was associated with vascular Density and Caliber measurements. These results are mainly attributable to their associations with GC-IPL and INL thickness. Additionally, the multidimensional relationships revealed by CCA demonstrate the complementary nature of the two sets of parameters and highlight their value as a composite biomarker for both ocular and systemic conditions. Moreover, Mendelian Randomization uncovered a bidirectional relationship between retinal layer thicknesses and vascular features. These findings provide preliminary insights into retinal neurovascular interactions; however, further research is necessary to elucidate their biological significance and potential clinical applications.

CRediT authorship contribution statement

Mayinuer Yusufu: Writing – original draft, Formal analysis,

Methodology. **Robert N. Weinreb:** Supervision, Writing – review & editing, Methodology. **Mengtian Kang:** Writing – review & editing, Formal analysis, Methodology. **Algis J. Vingrys:** Supervision, Writing – review & editing, Methodology, Conceptualization. **Xianwen Shang:** Supervision, Conceptualization, Writing – review & editing, Methodology. **Lei Zhang:** Supervision, Conceptualization, Writing – review & editing, Methodology. **Danli Shi:** Supervision, Conceptualization, Writing – review & editing, Investigation. **Mingguang He:** Supervision, Conceptualization, Writing – review & editing, Methodology.

Funding

This work was supported by the Global STEM Professorship Scheme (P0046113). The Centre for Eye Research Australia receives Operational Infrastructure Support from the Victorian State Government. M.Y. is supported by the Melbourne Research Scholarship established by the University of Melbourne. The funding source had no role in the design and conduct of the study; collection, management, analysis, and interpretation of the data; preparation, review, or approval of the manuscript; and decision to submit the manuscript for publication.

Declaration of competing interest

The authors declare that they have no known competing financial interests or personal relationships that could have appeared to influence the work reported in this paper.

Appendix A. Supplementary data

Supplementary data to this article can be found online at https://doi.org/10.1016/j.mvr.2025.104834.

Data availability

The authors do not have permission to share data.

References

Ames 3rd., A., 2000. CNS energy metabolism as related to function. Brain Res. Brain Res. Rev. 34 (1–2), 42–68.
Attwell, D., Iadecola, C., 2002. The neural basis of functional brain imaging signals. Trends Neurosci. 25 (12), 621–625.
Attwell, D., Buchan, A.M., Charpak, S., Lauritzen, M., MacVicar, B.A., Newman, E.A., 2010a. Glial and neuronal control of brain blood flow. Nature 468 (7321), 232–243.
Attwell, D., Buchan, A.M., Charpak, S., Lauritzen, M., Macvicar, B.A., Newman, E.A., 2010b. Glial and neuronal control of brain blood flow. Nature 468 (7321), 232–243.
Broe, R., Rasmussen, M.L., Frydkjaer-Olsen, U., et al., 2014. Retinal vessel calibers predict long-term microvascular complications in type 1 diabetes: the Danish Cohort of Pediatric Diabetes 1987 (DCPD1987). Diabetes 63 (11), 3906–3914.
Cabrera DeBuc, D., Somfai, G.M., Arthur, E., Kostic, M., Oropesa, S., Mendoza, Santiesteban C., 2018. Investigating Multimodal Diagnostic Eye Biomarkers of Cognitive Impairment by Measuring Vascular and Neurogenic Changes in the Retina. Front. Physiol. 9, 1721.
Chan, V.T.T., Sun, Z., Tang, S., et al., 2019. Spectral-Domain OCT Measurements in Alzheimer's Disease: A Systematic Review and Meta-analysis. Ophthalmology 126 (4), 497–510.
Chua, S.Y.L., Thomas, D., Allen, N., et al., 2019. Cohort profile: design and methods in the eye and vision consortium of UK Biobank. BMJ Open 9 (2), e025077.
Czako, C., Kovacs, T., Ungvari, Z., et al., 2020. Retinal biomarkers for Alzheimer's disease and vascular cognitive impairment and dementia (VCID): implication for early diagnosis and prognosis. Geroscience 42 (6), 1499–1525.
Edwards, M.M., McLeod, D.S., Li, R., et al., 2012. The deletion of Math5 disrupts retinal blood vessel and glial development in mice. Exp. Eye Res. 96 (1), 147–156.
Erskine, L., Herrera, E., 2014. Connecting the retina to the brain. ASN Neuro 6 (6).
Fu, Y., Yusufu, M., Wang, Y., He, M., Shi, D., Wang, R., 2023. Association of retinal microvascular density and complexity with incident coronary heart disease. Atherosclerosis 380, 117196.
Gardner, T.W., Davila, J.R., 2017. The neurovascular unit and the pathophysiologic basis of diabetic retinopathy. Graefes Arch. Clin. Exp. Ophthalmol. 255 (1), 1–6.
Girouard, H., Iadecola, C., 2006. Neurovascular coupling in the normal brain and in hypertension, stroke, and Alzheimer disease. J. Appl. Physiol. (1985) 100 (1), 328–335.
Hughes, A.D., Wong, T.Y., Witt, N., et al., 2009. Determinants of retinal microvascular architecture in normal subjects. Microcirculation 16 (2), 159–166.
Iadecola, C., 2013. The pathobiology of vascular dementia. Neuron 80 (4), 844–866.
Iadecola, C., 2017. The Neurovascular Unit Coming of Age: A Journey through Neurovascular Coupling in Health and Disease. Neuron 96 (1), 17–42.
Ko, F., Foster, P.J., Strouthidis, N.G., et al., 2017. Associations with Retinal Pigment Epithelium Thickness Measures in a Large Cohort: Results from the UK Biobank. Ophthalmology 124 (1), 105–117.
Kur, J., Newman, E.A., Chan-Ling, T., 2012. Cellular and physiological mechanisms underlying blood flow regulation in the retina and choroid in health and disease. Prog. Retin. Eye Res. 31 (5), 377–406.
Liew, G., Gopinath, B., White, A.J., Burlutsky, G., Yin Wong, T., Mitchell, P., 2021. Retinal Vasculature Fractal and Stroke Mortality. Stroke 52 (4), 1276–1282.
Loeffler, M., Engel, C., Ahnert, P., et al., 2015. The LIFE-Adult-Study: objectives and design of a population-based cohort study with 10,000 deeply phenotyped adults in Germany. BMC Public Health 15, 691.
London, A., Benhar, I., Schwartz, M., 2013. The retina as a window to the brain-from eye research to CNS disorders. Nat. Rev. Neurol. 9 (1), 44–53.
Normando, E.M., Davis, B.M., De Groef, L., et al., 2016. The retina as an early biomarker of neurodegeneration in a rotenone-induced model of Parkinson's disease: evidence for a neuroprotective effect of rosiglitazone in the eye and brain. Acta Neuropathol. Commun. 4 (1), 86.
Patel, P.J., Foster, P.J., Grossi, C.M., et al., 2016. Spectral-Domain Optical Coherence Tomography Imaging in 67 321 Adults: Associations with Macular Thickness in the UK Biobank Study. Ophthalmology 123 (4), 829–840.
Petzold, A., Balcer, L.J., Calabresi, P.A., et al., 2017. Retinal layer segmentation in multiple sclerosis: a systematic review and meta-analysis. Lancet Neurol. 16 (10), 797–812.
Pournaras, C.J., Rungger-Brändle, E., Riva, C.E., Hardarson, S.H., Stefansson, E., 2008. Regulation of retinal blood flow in health and disease. Prog. Retin. Eye Res. 27 (3), 284–330.
Sasongko, M.B., Wang, J.J., Donaghue, K.C., et al., 2010. Alterations in retinal microvascular geometry in young type 1 diabetes. Diabetes Care 33 (6), 1331–1336.
Satue, M., Obis, J., Rodrigo, M.J., et al., 2016. Optical Coherence Tomography as a Biomarker for Diagnosis, Progression, and Prognosis of Neurodegenerative Diseases. J. Ophthalmol. 2016, 8503859.
Selvam, S., Kumar, T., Fruttiger, M., 2018. Retinal vasculature development in health and disease. Prog. Retin. Eye Res. 63, 1–19.
Shi, D., Lin, Z., Wang, W., et al., 2022. A Deep Learning System for Fully Automated Retinal Vessel Measurement in High Throughput Image Analysis. Front. Cardiovasc. Med. 9, 823436.
Sudlow, C., Gallacher, J., Allen, N., et al., 2015. UK biobank: an open access resource for identifying the causes of a wide range of complex diseases of middle and old age. PLoS Med. 12 (3), e1001779.
Takusagawa, H.L., Liu, L., Ma, K.N., et al., 2017. Projection-Resolved Optical Coherence Tomography Angiography of Macular Retinal Circulation in Glaucoma. Ophthalmology 124 (11), 1589–1599.
Tien Yin Wong, F., Klein, Ronald, Tielsch, James M., Hubbard, Larry, Nieto, F. Javier, 2001. Retinal Microvascular Abnormalities and their Relationship with Hypertension, Cardiovascular Disease, and Mortality.
Wareham, L.K., Calkins, D.J., 2020. The Neurovascular Unit in Glaucomatous Neurodegeneration. Front. Cell Dev. Biol. 8, 452.
Wu, Z., Bogunović, H., Asgari, R., Schmidt-Erfurth, U., Guymer, R.H., 2021. Predicting Progression of Age-Related Macular Degeneration Using OCT and Fundus Photography. Ophthalmol. Retina 5 (2), 118–125.
Yang, Q., Reisman, C.A., Wang, Z., et al., 2010. Automated layer segmentation of macular OCT images using dual-scale gradient information. Opt. Express 18 (20), 21293–21307.
Yu, J., Gu, R., Zong, Y., et al., 2016. Relationship Between Retinal Perfusion and Retinal Thickness in Healthy Subjects: An Optical Coherence Tomography Angiography Study. Invest. Ophthalmol. Vis. Sci. 57 (9). Oct204–10.
Yusufu, M., Chen, Y., Dayimu, A., et al., 2024. Retinal Vascular Measurements and Mortality Risk: Evidence From the UK Biobank Study. Transl. Vis. Sci. Technol. 13 (1), 2.
Yusufu, M., Vingrys, A.J., Shang, X., et al., 2025. Population-based Normative Reference for Retinal Microvascular Atlas. Ophthalmol. Sci. 5 (3), 100723.
Zekavat, S.M., Raghu, V.K., Trinder, M., et al., 2022. Deep Learning of the Retina Enables Phenome- and Genome-Wide Analyses of the Microvasculature. Circulation 145 (2), 134–150.
Zekavat, S.M., Jorshery, S.D., Rauscher, F.G., et al., 2024. Phenome- and genome-wide analyses of retinal optical coherence tomography images identify links between ocular and systemic health. Sci. Transl. Med. 16 (731), eadg4517.